

Threading dislocation evolution in mega-electron-volt phosphorus implanted silicon

Craig Jasper^{a)} and Suman K. Banerjee

Motorola, Digital DNA Laboratory, 2200 West Broadway Road, Mesa, Arizona 85202

Allen Hoover

ON Semiconductors, 5005 East McDowell Road, Phoenix, Arizona 85008

Kevin S. Jones

Department of Materials Science and Engineering, SWAMP Center, University of Florida, Gainesville, Florida 32611

(Received 13 July 2000; accepted for publication 8 January 2001)

The effect of dose and energy on postannealing defect formation for high energy (mega-electron-volt) phosphorus implanted silicon has been studied using etch pit studies and transmission electron microscopy (TEM). Previous work has shown that after annealing there is a strong dependence of dislocation density threading to the surface on the implanted phosphorus dose and energy. A superlinear increase in threading dislocation density (TDD) with implant energy between 180 and 1500 keV is observed for a dose of $1 \times 10^{14} \text{ cm}^{-2}$. In addition as a function of ion fluence, there is a maximum in the threading dislocation density at a dose of $1 \times 10^{14} \text{ cm}^{-2}$ followed by a rapid decrease in TDD. Both the superlinear increase in TDD with increasing energy and the rapid decrease with increasing dose have been further investigated by TEM. A TEM study of these higher doses revealed formation of a strong bimodal loop distribution with small loops averaging $<1000 \text{ \AA}$ and large loops averaging around $1 \mu\text{m}$ in size. Over the dose range of $1 \times 10^{14} \text{ cm}^{-2}$ to $5 \times 10^{14} \text{ cm}^{-2}$, the superlinear decrease in TDD from $1 \times 10^6 \text{ cm}^{-2}$ to $<1 \times 10^4 \text{ cm}^{-2}$ coincides with the superlinear increase in small dislocation loops from below $1 \times 10^6 \text{ cm}^{-2}$ to above $1 \times 10^{10} \text{ cm}^{-2}$. It is suggested that the homogeneous nucleation theory can explain many of the results. However, the chemical presence of phosphorus appears to also play an important role in the formation of the small dislocation loops and possibly threading dislocations. © 2001 American Institute of Physics. [DOI: 10.1063/1.1351865]

I. INTRODUCTION

High energy ion implantation processes are becoming increasingly important in the manufacture of silicon based semiconductor devices. The manufacturing processes include formation of buried collectors in complementary metal-oxide-semiconductors with bipolar (BiCMOS) devices¹ proximity gettering centers,² and profiled tubs or wells.³ However, severe lattice defects can be generated in the region near the projected range (R_p) of the implanted impurities.⁴ Etch pit densities, plan-view and cross-sectional transmission electron microscopy (TEM) studies of the silicon substrate have shown the existence of defects that originate at the projected range of the implant and extend all the way to the surface of the silicon substrate.⁵⁻⁸ These extended defects, which are known as “threading dislocations,”⁵ appear to be responsible for high leakage currents in n^+/p and p^+/n junction diodes fabricated above high energy boron and phosphorus implanted layers.^{3,9} Therefore, a fundamental understanding of the physical phenomena that contribute to the formation of threading dislocations is essential prior to incorporating high energy ion implantation into the fabrication of silicon based semiconductor devices. The goal of this

article is to show how competing extended defect formation mechanisms interact to affect threading dislocation formation.

II. EXPERIMENT

Extended defect formation was studied for a range of doses and high energy (mega-electron-volt) implant conditions followed by a low temperature anneal. Etch pit densities, plan-view and cross-sectional TEM were used to characterize the type, depth, and concentration of dislocations in the material. The implants were carried out in $7\text{-}\mu\text{m}$ -thick lightly doped ($1 \times 10^{15} \text{ cm}^{-3}$) p -type epitaxial silicon grown on (100) p^+ silicon. Phosphorus implant energies were varied from 180 to 5000 keV, at various doses, ranging from 1×10^{13} to $5 \times 10^{14} \text{ cm}^{-2}$. After implantation the samples were annealed at 800°C for 90 min followed by a 550°C anneal for 60 min and finally a 950°C anneal for 10 min, to emulate some of the thermal cycles of an advanced CMOS process. Etch pit samples were produced using a Schimmel etch consisting of a 2:14 9% HF:1 M CrO_3 solution. An etch of 20 s was used.

To examine the projected range defects both plan-view and cross-sectional TEM were done on the samples after annealing. The plan-view samples were prethinned (when necessary) using chemical mechanical touch polishing

^{a)}Electronic mail: rxtp20@email.sps.mot.com

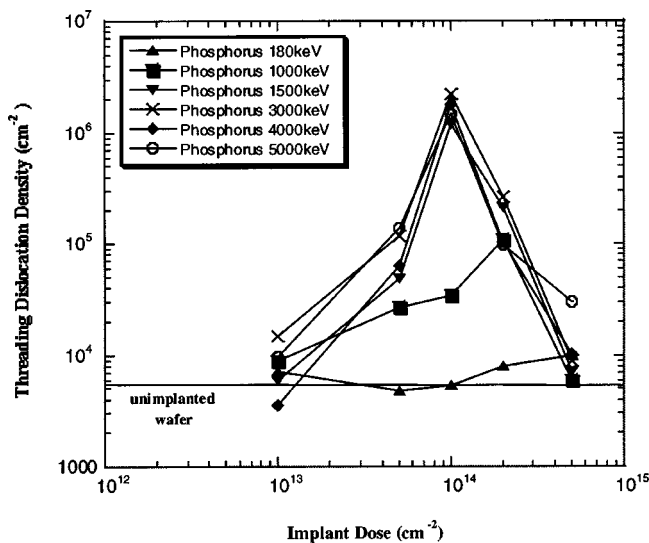


FIG. 1. Results of etch pits density counts of the threading dislocation density for varying doses and energies of mega-electron-volt phosphorus implanted samples after annealing. A peak threading dislocation density is shown to be at a dose of approximately $1 \times 10^{14} \text{ cm}^{-2}$.

(CMP) with a silica slurry, to position the peak of the projected range damage approximately 3000–4000 Å below the surface. A high-resolution TEM operating at 200 kV was used to study the projected range defects in plan view. Micrographs were taken using bright field g_{220} imaging conditions. These conditions allow one to observe defects as deep as 5000–10 000 Å deep. TEM of unimplanted control samples show that the CMP process does not introduce any observable defects.

III. RESULTS

Figure 1 depicts the results from etch pit studies of the surface threading dislocation density (TDD) for varying energies of phosphorus implants. The background threading dislocation density of $5 \times 10^3 \text{ cm}^{-2}$ was obtained by etching an unimplanted sample wafer. Two distinct effects are seen from the figure. First, there exists the effect of implant dose. For implant energies greater than 1500 keV, the surface threading dislocation density increases from near background density levels ($\sim 5 \times 10^3 \text{ cm}^{-2}$) for an implant dose of $1 \times 10^{13} \text{ cm}^{-2}$ to a maximum of $\sim 2 \times 10^6 \text{ cm}^{-2}$ for an implant dose of $1 \times 10^{14} \text{ cm}^{-2}$. For implant doses greater than $1 \times 10^{14} \text{ cm}^{-2}$ the TDD levels start decreasing. Therefore, the TDD level appears to saturate at $\sim 2 \times 10^6 \text{ cm}^{-2}$ for an implant dose of $1 \times 10^{14} \text{ cm}^{-2}$. The second effect is the effect of energy. The trend in TDD levels discussed earlier is seen only for implant energies greater than 1500 keV. For all the energies from 1500 to 5000 keV studied, the trends were remarkably similar with a near identical TDD saturation level of $2 \times 10^6 \text{ cm}^{-2}$ achieved at an implant dose of $1 \times 10^{14} \text{ cm}^{-2}$. However, for implant energies less than 1500 keV no such clear trends are visible. In fact, for an implant energy of 180 keV the TDD level seems to remain near constant and below $1 \times 10^4 \text{ cm}^{-2}$.

To understand the decrease in TDD levels for phosphorus implant doses greater than $1 \times 10^{14} \text{ cm}^{-2}$, a series of

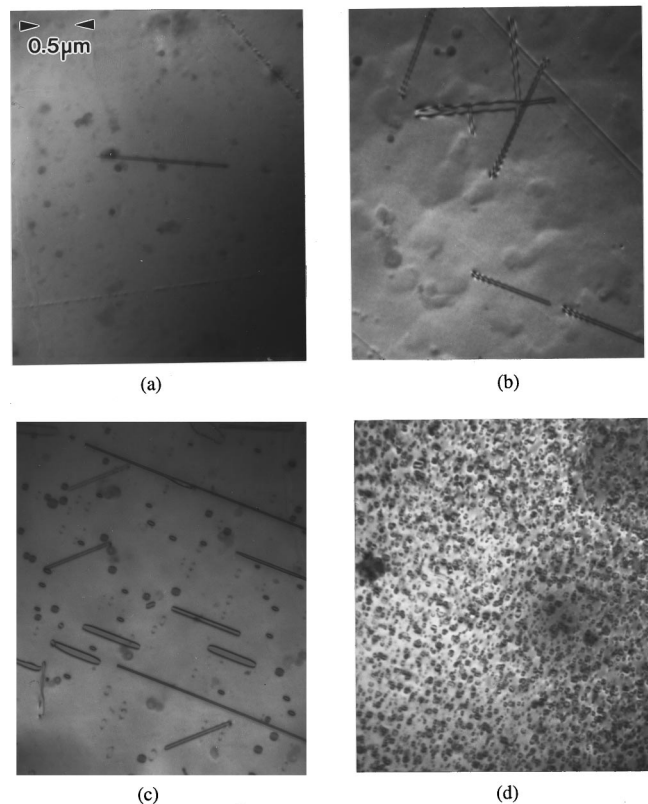


FIG. 2. Plan-view TEM micrographs of phosphorus implanted samples at varying doses at 1500 keV and annealed. (a) Phosphorus dose $5 \times 10^{13} \text{ cm}^{-2}$, (b) phosphorus dose $1 \times 10^{14} \text{ cm}^{-2}$, (c) phosphorus dose $2 \times 10^{14} \text{ cm}^{-2}$, (d) and phosphorus dose $5 \times 10^{14} \text{ cm}^{-2}$. The micrographs show the evolution of dislocations at various doses for a constant energy. Note the large increase in small dislocation loops with increasing dose.

TEM studies was done. Four different implant energies (180 keV, 1.5, 2.5, and 5 MeV) and four different doses (5×10^{13} , 1×10^{14} , 2×10^{14} , and $5 \times 10^{14} \text{ cm}^{-2}$) were chosen for this TEM study. Figure 2 shows the TEM results of the 1500 keV phosphorus implant at four different doses after annealing. Because of the use of a CMP process to thin the samples, the defects shown are those at the projected range of the implant. These micrographs are indicative of the evolution of defects for most of the high energy implants studied. The density of defects can be quantified by taking micrographs of several different regions and counting each image after printing. It is clear there is a rapid increase in the density of the defects upon annealing. Figure 3 shows a graph of the total dislocation loop density determined from TEM versus the implant dose. Cross-sectional TEM confirmed the defects were in a band around the projected range of the implants. For the implants at various energy levels (180, 1500, 2500, and 5000 keV), the total defect density increases from $\sim 1 \times 10^7 \text{ cm}^{-2}$ to $\sim 1 \times 10^{10} \text{ cm}^{-2}$. From Figs. 1 and 3, we can see that beyond an implant dose of $1 \times 10^{14} \text{ cm}^{-2}$ there is an increase in the total defect density concentration, but there is a decrease in the TDD concentration. This implies that the surface threading dislocations may be evolving into another form of dislocation loop that does not thread to the surface.

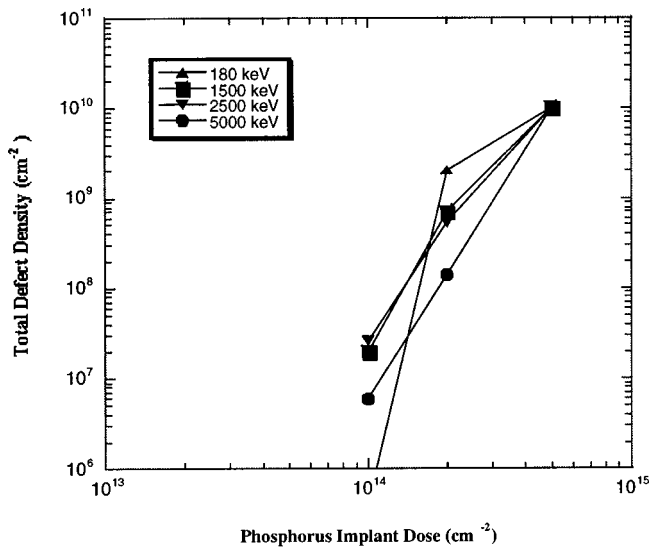


FIG. 3. The total defect density dependence on dose is shown. Beyond a dose of $1 \times 10^{14} \text{ cm}^{-2}$ there is a superlinear increase in the total concentration of defects from $\sim 1 \times 10^7 \text{ cm}^{-2}$ to $\sim 1 \times 10^{10} \text{ cm}^{-2}$.

TEM micrographs were analyzed at different doses and energies to extract the average diameter of these dislocation loops. Figure 4 is a plot of the average diameter of the dislocation loops at various energy levels (180, 1500, 2500, and 5000 keV) for implant doses greater than $1 \times 10^{14} \text{ cm}^{-2}$. This plot shows a superlinear decrease in the average loop diameter with an increasing implant dose. These results would support the hypothesis that the surface threading dislocations are evolving into smaller dislocation loops for implant doses greater than $1 \times 10^{14} \text{ cm}^{-2}$.

The size distribution behaves in a very unexpected fashion. With increasing dose rather than getting a simple decrease in the average diameter, the system actually develops

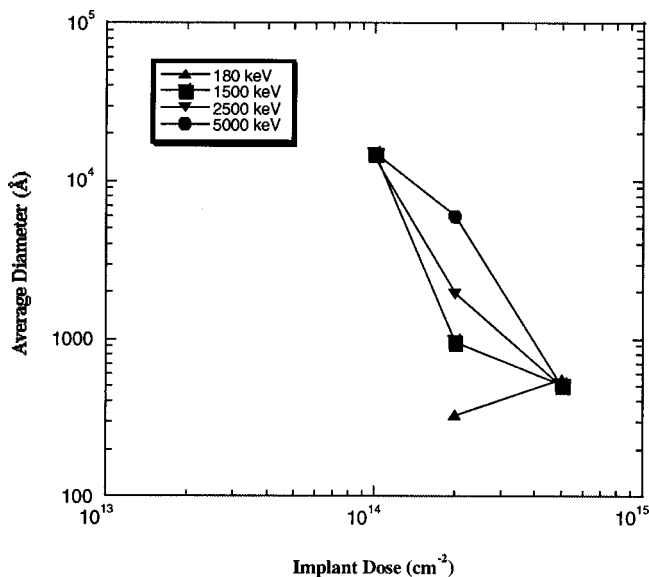


FIG. 4. The average diameter of the dislocation loops at various energy levels (180, 1500, 2500, and 5000 keV) for implant doses greater than $1 \times 10^{14} \text{ cm}^{-2}$. This plot shows a linear decrease in the average loop diameter with an increase in the implanted dose.

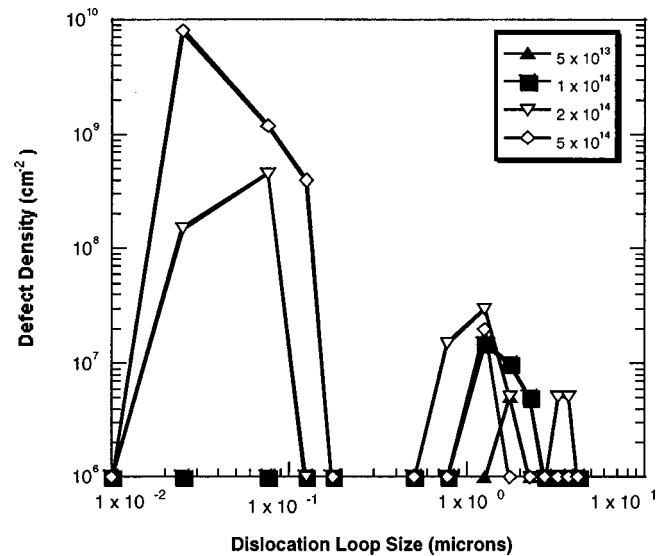


FIG. 5. Size distribution of the 1500 keV phosphorus implanted samples as a function of implant dose after annealing. Note the formation of a bimodal distribution with increasing dose.

a bimodal loop distribution. This can be seen in Fig. 5 for the 1500 keV phosphorus implanted samples as a function of dose. At low doses (the solid symbols) the only defects observed by TEM are the large loops. However, with increasing dose a high density of very small dislocation loops forms. In order to further analyze the effect of energy and dose on this bimodal distribution, the dislocation loops have been grouped into two different sizes, large loops ($>1500 \text{ \AA}$) and small loops ($<1500 \text{ \AA}$). The classification of large loops as being greater than 1500 \AA and small loops being less than 1500 \AA is arbitrary. However, there is a clear bimodal distribution in defect sizes and in general the small loops are on average about 500 \AA in diameter and the large loops are on average around a micron in length.

Figure 6 shows the density of large dislocation loops ($>1500 \text{ \AA}$) as a function of the phosphorus implant dose for different implant energies. For an implant energy of 180 keV, the density of large loops is $\sim 1 \times 10^6 \text{ cm}^{-2}$, which is at the TEM detection limit. However, for the other implant energies studied, the large dislocation loop density increases from $5 \times 10^6 \text{ cm}^{-2}$ for an implant dose of $5 \times 10^{13} \text{ cm}^{-2}$ to a maximum value of $\sim 7 \times 10^7 \text{ cm}^{-2}$ at an implant dose of $2 \times 10^{14} \text{ cm}^{-2}$. For implant doses greater than $2 \times 10^{14} \text{ cm}^{-2}$ the large dislocation loop density remains nearly constant at a value of $\sim 7 \times 10^7 \text{ cm}^{-2}$. These results show that there is a weaker dependence on dose for the formation of large dislocation loops and there is even a possible decrease in their density for higher doses.

Figure 7 shows a graph of the density of small dislocation loops ($<1500 \text{ \AA}$) as a function of the phosphorus implant dose. For doses $\leq 1 \times 10^{14} \text{ cm}^{-2}$ the density of small dislocation loops is below the detection limit. However, the small dislocation loop density increases at least two to three orders of magnitude when the implant dose is simply doubled from 1×10^{14} to $2 \times 10^{14} \text{ cm}^{-2}$. An additional one to two orders of magnitude increase is observed when the dose is increased from 2×10^{14} to $5 \times 10^{14} \text{ cm}^{-2}$. Thus, there is a

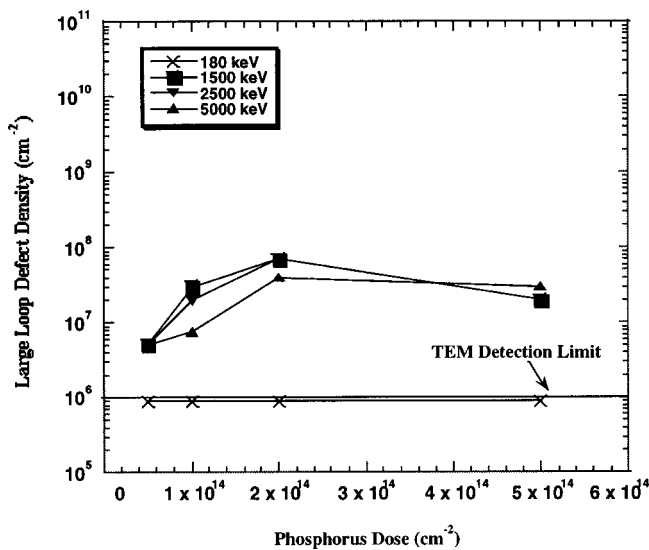


FIG. 6. Plan-view TEM results of the large (>1500 Å) dislocation loop density in phosphorus implanted samples after annealing as a function of implant dose for various implant energies. The large defects show some increase followed by a slight decrease in density with increasing dose.

superlinear increase in the density of small dislocation loops with increasing dose. Figure 1 showed that the surface threading dislocation density reaches a maximum for an implant dose of $1 \times 10^{14} \text{ cm}^{-2}$ and then showed a superlinear decrease in density for doses between $1 \times 10^{14} \text{ cm}^{-2}$ and $5 \times 10^{14} \text{ cm}^{-2}$. This suggests there could be correlation between the formation of small dislocation loops and the decrease in threading dislocations.

IV. DISCUSSION

In order to explain the results observed in Figs. 1–7 it is important to examine what theories have been previously proposed to explain the correlation of threading dislocations

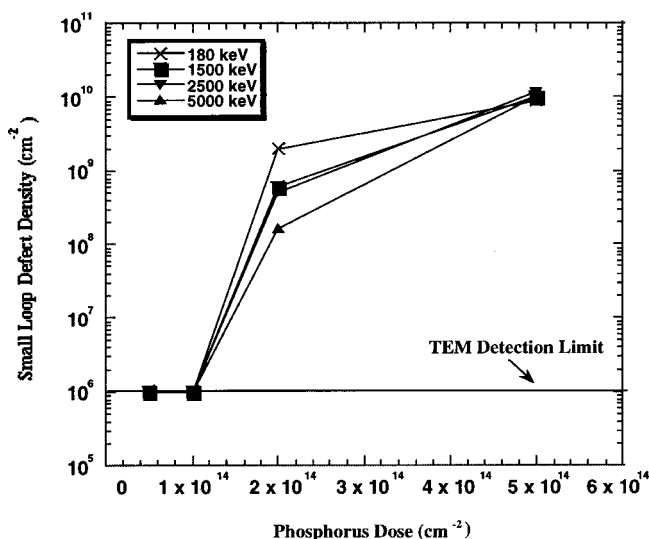


FIG. 7. Plan-view TEM results of the small (<1500 Å) dislocation loop density in phosphorus implanted samples after annealing as a function of implant dose for various implant energies. Note the superlinear increase in defect density with increasing dose.

on implant conditions. Cheng *et al.*⁵ proposed a simple model for the decrease in threading dislocation with increasing dose above $1 \times 10^{14} \text{ cm}^{-2}$. They proposed that as the dose increases the average size of the defect decreases and thus the threading dislocations no longer reach the surface. The primary source of interstitials for their model is the contribution from the implanted dose (so-called “plus” factor).¹⁰ This model, which is in effect homogeneous nucleation theory,¹¹ offers the simplest approach to understanding the loop nucleation kinetics. It has been shown that excess interstitials in silicon will precipitate into extended defects called $\{311\}$ defects.¹² It has also been shown that these $\{311\}$ defects can transform into dislocation loops.¹³ The shape of the large dislocation loops and their size are both consistent with the threading dislocations forming from the transformation (presumably unfauling) of isolated large $\{311\}$ defects.^{5,6,14}

Figure 3 shows that there is a clear superlinear increase in defect density with dose and that the average size of the defects does indeed decrease with increasing dose as observed in Fig. 4. Thus, this model on the surface works for these results. One complicating factor is the observation in Fig. 1, where the defect density behavior as a function of dose is very similar for implant energies between 1500 and 5000 keV. If the simple model is used then the plus concentration for these various energies is the same so one would expect the higher energy implants to have fewer threading dislocations simply because they are deeper. These results imply that the increase in defect depth with increasing implant energy must be off-set by the increase in defect size. This in turn means that there are fewer defects at higher energies which is possibly seen in Fig. 7. Therefore, either the average size is larger or there are more interstitials available to make the defects larger and thus reach the surface. More interstitials could form because of Frenkel pair separation.

Frenkel pair separation is a well documented source of excess interstitial for higher energy implants into Si. It has been shown that for mega-electron-volt implants the separation can lead to an excess vacancy population near the surface and a higher interstitial population around the projected range of the implant.^{15–17} Thus, the observation that there is a very weak energy dependence suggests a second source of interstitials above the simple plus one concentration may contribute. Additional low temperature experiments would need to be done to quantify the trapped interstitials in the $\{311\}$ defects before this could be verified.

Another complication from the simple model arises because of bimodal loop distribution that is observed in Fig. 5. This arises because of the saturation in large loops shown in Fig. 6 and the rapid increase in small loops in Fig. 7 with increasing dose. This bimodal distribution suggests a more complicated mechanism than simple homogeneous nucleation is involved. One possibility is that there are two mechanisms for loop formation. It has been shown¹⁸ that transformation of $\{311\}$ defects into dislocation loops, presumably through unfauling, can account for a significant fraction of the dislocation loops that form upon annealing. However, it was also pointed out^{18,19} that many of the dislocation loops

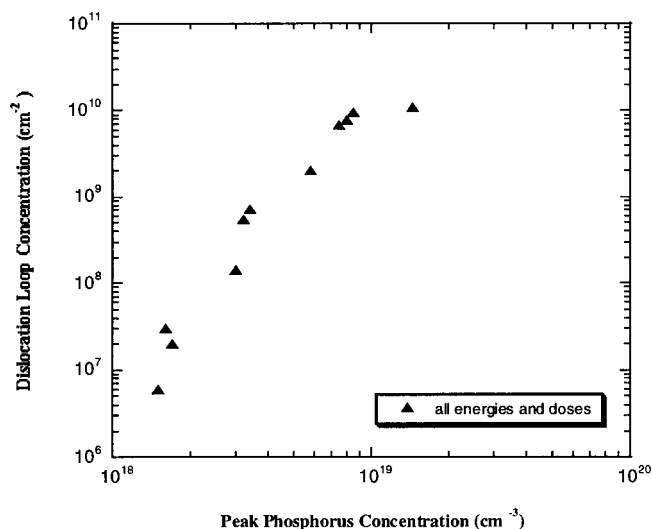


FIG. 8. The dependence of the dislocation loop concentration on the peak phosphorus concentration for all of the samples examined in this study. The strong correlation is consistent with phosphorus having a chemical species effect on loop nucleation.

form prior to the observation of visible transformation from {311} defects. Thus, it is possible that the bimodal distribution observed arises because at low doses the mechanism involving transformation of {311} defects to loops dominates, whereas at higher doses a “direct” formation of loops without involving {311} defects dominates at some submicroscopic cluster regime. It is impossible at this time to rule out this alternative pathway because it is not possible to observe this possible submicroscopic transformation.

A second possibility to explain the bimodal loop distribution is that the concentration of phosphorus is affecting the loop formation process. Keys *et al.*²⁰ has shown using phosphorus wells and Si⁺ implants, that with increasing phosphorus concentration there is a tendency to reduce the formation of {311} defects and increase the formation of small dislocation loops. More recently this effect was shown to track with the so called “kink” concentration in the phosphorus diffusion profiles.²⁰ This phosphorus was shown to start increasing the loop formation process at a phosphorus concentration approximately one order of magnitude below the kink concentration. For the first anneal in this study (800 °C), the kink concentration is approximately $2 \times 10^{19} \text{ cm}^{-2}$.²¹

To further investigate this possibility the total dislocation loop concentration extracted from TEM micrographs was plotted versus the peak phosphorus concentration determined by secondary ion mass spectrometry for all the energies and doses in this study in Fig. 8. The peak phosphorus concentration was used since these are nonamorphizing implants. This figure shows that the total dislocation loop concentration increases dramatically for phosphorus concentrations between $1 \times 10^{18} \text{ cm}^{-2}$ and $2 \times 10^{19} \text{ cm}^{-2}$ (approximately an order of magnitude below the kink concentration). Thus, the concentration of phosphorus is in the correct range to be affecting the loop formation process. The mechanism by which phosphorus enhances loop formation is not yet understood but the effect is well documented. Without mega-

electron-volt Si⁺ implants for comparison it cannot be conclusively stated that the phosphorus is affecting the loop distribution, however, the correlation in Fig. 8 suggests this mechanism may be significant. Further experiments with Si⁺ implants are in progress.

V. CONCLUSION

In conclusion, for high energy phosphorus implants there appears to be a direct correlation between the decrease in threading dislocation density with increasing dose and the increase in dislocation density at the projected range. The results show a weak energy dependence above a certain energy threshold. TEM studies reveal the formation of a bimodal dislocation loop distribution of small and large loops. These large loops start to appear at an implant dose of $5 \times 10^{13} \text{ cm}^{-2}$ and increase in density from $5 \times 10^6 \text{ cm}^{-2}$ to a maximum of $6 \times 10^7 \text{ cm}^{-2}$ at a dose of $2 \times 10^{14} \text{ cm}^{-2}$. With further increases in the dose the density of large loops decrease gradually to $3 \times 10^7 \text{ cm}^{-2}$ at a dose of $5 \times 10^{14} \text{ cm}^{-2}$. The small loops are below TEM detection limits until a dose of $2 \times 10^{14} \text{ cm}^{-2}$ when they appear at a density of $\sim 5 \times 10^8 \text{ cm}^{-2}$. With increasing the dose the small loop density exhibits a superlinear increase in density to $1 \times 10^{10} \text{ cm}^{-2}$ for a dose of $5 \times 10^{14} \text{ cm}^{-2}$. The superlinear increase in the formation of small dislocation loops coincides with the superlinear decrease in threading dislocation density. It is suggested that understanding the energy, dose, and loop size distribution dependence of the threading dislocations requires understanding the sources of interstitials and the loop nucleation kinetics. The presence of phosphorus may play a significant role in the formation of dislocation loops and thus threading dislocations.

ACKNOWLEDGMENTS

The authors would like to thank the Implant Group in Advanced Custom Technologies for the numerous hours that they have spent on preparing and running the many samples that it took to generate the data for this article. The authors would also like to thank Britta Elyse Jones, Ryan Scott Jones, and Sean Michael Jones for their assistance with the data analysis.

- ¹A. Tamba, T. Kobayashi, and T. Suzuki, *Jpn. J. Appl. Phys., Part 1* **31**, 156 (1992).
- ²H. Wong, N. W. Cheung, P. K. Chu, J. Liu, and J. W. Mayer, *Appl. Phys. Lett.* **52**, 1023 (1988).
- ³K. Tsukamoto, S. Komori, T. Kuroi, and Y. Akasaka, *Nucl. Instrum. Methods Phys. Res. B* **59**, 584 (1991).
- ⁴J. Washburn, *Mater. Res. Soc. Symp. Proc.* **2**, 209 (1980).
- ⁵J. Y. Cheng, D. J. Eaglesham, D. C. Jacobson, P. A. Stolck, J. L. Benton, and J. M. Poate, *J. Appl. Phys.* **80**, 2105 (1996).
- ⁶C. Jasper, A. Hoover, and K. S. Jones, *Appl. Phys. Lett.* **75**, 2629 (1999).
- ⁷K. K. Bourdelle, D. J. Eaglesham, D. C. Jacobson, and J. M. Poate, *J. Appl. Phys.* **86**, 1221 (1999).
- ⁸K. K. Bourdelle, D. J. Eaglesham, D. C. Jacobson, and J. M. Poate, *J. Electrochem. Soc.* **98**, 584 (1999).
- ⁹H. Sayama, M. Takai, Y. Akasaka, K. Tsukamoto, and S. Namba, *J. Appl. Phys.* **28**, 1673 (1989).
- ¹⁰M. D. Giles, *J. Electrochem. Soc.* **138**, 1160 (1991).
- ¹¹M. Volmer and A. Weber, *J. Phys. Chem.* **119**, 227 (1926).
- ¹²T. Y. Tan, *Philos. Mag.* **44**, 101 (1981).
- ¹³D. J. Eaglesham, P. A. Stolck, H.-J. Gossmann, T. E. Haynes, and J. M.

- Poate, Nucl. Instrum. Methods Phys. Res. B **106**, 191 (1995).
- ¹⁴D. J. Eaglesham, P. A. Stolk, H.-J. Gossmann, and J. M. Poate, Appl. Phys. Lett. **65**, 2305 (1994).
- ¹⁵S. Coffa, V. Privitera, F. Priolo, S. Libertino, and G. Mannino, J. Appl. Phys. **81**, 1639 (1997).
- ¹⁶V. C. Venezia, T. E. Haynes, A. Agarwal, L. Pelaz, H.-J. Gossmann, D. C. Jacobsons, and D. J. Eaglesham, Appl. Phys. Lett. **74**, 1299 (1999).
- ¹⁷V. C. Venezia, D. J. Eaglesham, T. E. Haynes, A. Agarwal, D. C. Jacobson, H.-J. Gossmann, and F. H. Baumann, Appl. Phys. Lett. **73**, 2980 (1998).
- ¹⁸J. Li and K. S. Jones, Appl. Phys. Lett. **73**, 3748 (1998).
- ¹⁹L. S. Robertson, K. S. Jones, L. M. Rubin, and J. Jackson, J. Appl. Phys. **87**, 2910 (2000).
- ²⁰P. H. Keys, J. H. Li, E. Heitman, M. E. Law, K. S. Jones, and P. Packan, Mater. Res. Soc. Symp. Proc. **568**, 199 (1999).
- ²¹F. N. Schwettmann and D. L. Kendall, Appl. Phys. Lett. **21**, 2 (1972).